Materials Today Chemistry 29 (2023) 101443

Contents lists available at ScienceDirect

Materials Today Chemistry

journal homepage: www.journals.elsevier.com/materials-today-chemistry/

Adsorbate/adsorbent interactions in microporous zeolites: mechanistic insights from NMR relaxation and DFT calculations

C. D'Agostino [a, b, *], P. Bräuer [c], J. Zheng [d], N. Robinson [e], A.P.E. York [f], L. Song [d], X. Fan [a, g, **]

[a] Department of Chemical Engineering, The University of Manchester, Engineering Building A, Oxford Road, Manchester, M13 9PL, UK
[b] Dipartimento di Ingegneria Civile, Chimica, Ambientale e Dei Materiali (DICAM), Alma Mater Studiorum — Università di Bologna, Via Terracini, 28, 40131, Bologna, Italy
[c] Department of Chemical Engineering and Biotechnology, University of Cambridge, Philippa Fawcett Drive, West Cambridge Site, Cambridge, CB3 0AS, UK
[d] College of Chemistry and Chemical Engineering, China University of Petroleum (East China), Qingdao, 266555, Shandong, China
[e] Department of Chemical Engineering, University of Western Australia, 35 Stirling Highway, Perth, WA, 6009, Australia
[f] Johnson Matthey Technology Centre, Blount's Court, Sonning Common, Reading, RG4 9NH, UK
[g] Nottingham Ningbo China Beacons of Excellence Research and Innovation Institute, University of Nottingham Ningbo China, 211 Xingguang Road, Ningbo, 315100, China

ARTICLE INFO

Article history:
Received 6 November 2022
Received in revised form
12 January 2023
Accepted 10 February 2023
Available online xxx

Keywords:
Nuclear magnetic resonance spectroscopy
ZSM-5
Silica-to-alumina ratio (SAR)
Adsorption
Density functional theory (DFT)

ABSTRACT

Nuclear magnetic resonance (NMR) relaxation is an effective and non-invasive technique for probing guest-host interactions in porous materials. In particular, the ratio of longitudinal-to-transverse nuclear spin relaxation time constants T_1/T_2 has been demonstrated as a robust indicator of adsorbate/adsorbent interactions in mesoporous media. However, the use of NMR relaxation times in microporous materials to probe interactions and dynamics remains relatively unexplored. Herein, we investigate and describe the effect of the aluminium content in microporous HZSM-5 zeolites on the NMR relaxation times of a range of common liquid probe molecules. In particular, we discuss the NMR relaxation time behavior of liquids with hydrophilic (water, methanol) and hydrophobic (toluene, methyl cyclohexane) properties adsorbed over HZSM-5 samples with varying silica-to-alumina ratios (SAR = SiO_2/Al_2O_3). Our results demonstrate that highly polar molecules show high sensitivity to aluminium content (i.e., surface acidity), with T_1/T_2 ratios increasing significantly for higher acidity zeolites. Conversely, for molecules with low polarity, the T_1/T_2 ratio as a function of SAR remains approximately constant, and in the zeolites with low SAR is much lower compared to that of water and methanol. Density functional theory (DFT) calculations are employed to contrast the surface interaction mechanisms of water and toluene within model zeolite structures of varying SAR, and provide molecular level insights into the observed trends in NMR relaxation behavior.

© 2023 The Author(s). Published by Elsevier Ltd. This is an open access article under the CC BY license (http://creativecommons.org/licenses/by/4.0/).

1. Introduction

Understanding and quantifying the adsorption of molecules in microporous zeolites is crucial to their application across industrial processes, such as separation and catalysis [1–3]. For example, knowledge of adsorption properties is necessary to select appropriate zeolites for efficient and cost-effective separations or catalytic reactions. Several methods have been developed to probe adsorption over zeolites, most notably infrared spectroscopy (IR) [4,5], temperature-programmed desorption (TPD) [6,7], and calorimetry [8,9]. Reactive gas chromatography has also been recently reported for quantification of zeolite acidity using the alkylamine decomposition as a probe reaction [10].

In recent years, NMR protocols for studying adsorption and dynamics of bulk fluids and fluids in porous materials have been developed [11–14]. In particular, NMR relaxation time analysis has emerged as a rapid and non-invasive probe of the adsorbate/adsorbent surface interactions of fluids inside porous materials, in particular inorganic porous materials used for catalytic applications [15–22]. For mesoporous structures, it has been demonstrated that the ratio of longitudinal (T_1) and transverse (T_2) relaxation times, T_1/T_2, is a novel indicator of adsorbate/adsorbent affinity, which can

* Corresponding author.
** Corresponding author.
E-mail addresses: carmine.dagostino@manchester.ac.uk (C. D'Agostino), xiaolei.fan@manchester.ac.uk (X. Fan).

https://doi.org/10.1016/j.mtchem.2023.101443
2468-5194/© 2023 The Author(s). Published by Elsevier Ltd. This is an open access article under the CC BY license (http://creativecommons.org/licenses/by/4.0/).

be related to an energy of adsorption [23,24]. The acquisition of this metric has been previously used to investigate solvent and product inhibition over mesoporous metal oxide catalysts [25–28]. Habina and Krzyżak [29] have used the T1/T2 ratio to quantify water interaction in mesoporous silica samples, in particular MCM-41 and SBA-15, concluding that the presence of surface defects in SBA-15 leads to stronger surface interactions. A further recent study focused on the use of deuteron NMR at variable temperatures to study the molecular dynamics of deuterated molecules confined to FAU X and Y zeolites [30], suggesting that decreased mobility can be caused by an increase in surface interactions, which were related to the quadrupolar properties of the adsorbed species.

While this concept has been established for mesoporous materials (with pore sizes 2–50 nm according to the International Union of Pure and Applied Chemistry (IUPAC) classification), the relationship between NMR relaxation times, in particular the T_1/T_2 NMR ratio, and adsorbate/adsorbent interactions in microporous materials (with pore sizes <2 nm according to the IUPAC classification), such as pristine zeolites, remains largely unexplored. There has been previous work on partially microporous polymers, whereby the T_1/T_2 ratio for adsorbed water was shown to present variations in the range of 25–125 as a function of hydroxyl group density on the polymer mesh [31]. Fast field cycling (FFC) NMR has also been used to study relaxation behavior in micro/mesopores, whereby different adsorption regimes could be observed [32]. A total observable dispersion (TOD) parameter was also introduced to characterize surface interactions in fast field cycling (FFC) NMR studies of adsorption dynamics in porous materials [33,34].

Recently, a newly reported study from Robinson et al. [35] has shown that a clear relationship exists between the T_1/T_2 ratio of pyridine (measured at high field, that is, 300 MHz) confined within MFI HZSM-5 zeolites and the silica/alumina ratio (SAR) of these zeolites, the latter being indicative of material acidity. In particular, a decrease in SAR (i.e., an increase in zeolite acidity) was shown to correlate very well with an increase in T_1/T_2 of the probe pyridine molecule confined within the zeolite pore space, suggesting that NMR relaxation time analysis can be a valuable tool for the non-invasive characterization of adsorption phenomena in microporous solids. An extension of this methodology, for probing surface interactions and confinement effects in zeolites, to low-field, bench-top NMR has also been demonstrated [36]. This recently reported findings represent the first studies to systematically investigate the application of NMR relaxation time analysis to probe the effect of zeolite acidity on interactions with confined molecules.

Prompted by these initial findings, we report here the NMR relaxation behavior of common polar and apolar molecules within HZSM-5 exhibiting a range of different acidic properties, tuned by changing the silica/alumina ratio (SAR = $SiO_2/Al2O_3$) of the material. As probe species, water and methanol were selected as highly polar probe molecules, while toluene and methyl cyclohexane were chosen as species exhibiting apolar characteristics. Our NMR data is supported by atomistic modelling performed using density functional theory (DFT) calculations, which we employ here to explore the interaction mechanisms of example polar/apolar adsorbates within the model zeolite structures.

2. Experimental

2.1. Materials and chemicals

Methanol (99.8%) and methyl cyclohexane (≥99%) were obtained from Sigma Aldrich. Toluene (≥99.5%) was obtained from Alfa Aesar. Deionised water was obtained from a laboratory water purification system (Elga Purelab). All chemicals were used as supplied. ZSM5 samples (with typical pore diameters in the range 5–6 Å) with various SAR (defined here as SiO_2/Al_2O_3) values, 23, 30, 50 and 80, were purchased from Alfa Aesar (in NH_4^+ form) as powders. These samples were calcined in a furnace with synthetic air (100 cm^3/min, Air Liquide) at 773 K for 4 h to convert them to the H^+ form HZSM-5; heating and cooling were carried out at 5 K/min. Samples are named according to their SAR values, as supplied by Alfa Aesar, and denoted as HZSM-5 (SAR). The SAR values were converted to Al concentration per unit cell (Al u.c.) using the chemical formula of HZSM-5 ($H_nAl_nSi_{96-n}O_{192} \times 16H_2O$) giving the conversion equation Al u.c. = 96/(1 + SAR/2) [37].

Samples for NMR analysis were prepared by pressing zeolite powder into tablets using a manual hydraulic press; a 2 tonne compressive force was applied to approximately 250 mg of powder in each case, forming cylindrical tablets measuring around 13 mm in diameter and 1 mm in thickness. The tablets were then broken into approximately 10 mg pieces so as to fit within a standard 5 mm NMR tube.

2.2. NMR experiments

NMR experiments were performed at 298 K on a Bruker DMX 300 spectrometer operating at a ^1H frequency of 300.13 MHz. Samples were prepared by soaking the HZSM-5 solid in the liquid under investigation, that is, water, methanol, toluene and methyl cyclohexane, for at least 24 h. The solids were then dried on a pre-soaked filter paper to remove any excess liquid on the external surface, and finally transferred to 5 mm NMR tubes. To ensure a saturated atmosphere in the NMR tube, thus minimizing errors due to evaporation of liquid, a small amount of liquid was placed onto absorbent filter paper, which was then placed under the cap of the NMR tube, with the latter sealed with parafilm. The sample tube was finally placed into the magnet and left for approximately 20 min before starting the measurements to achieve thermal equilibrium.

NMR relaxation data was acquired using a 2D $T_1 - T_2$ pulse sequence described in detail elsewhere [38], and shown schematically in Fig. 1. A 180° radiofrequency (*RF*) excitation pulse first rotates the spin magnetization onto the $-z$ axis. The magnetization then relaxes longitudinally back towards thermal equilibrium for a time τ_1, with relaxation occurring along the z axis, which is aligned with the static external magnetic field. A 90° *RF* pulse rotates the spin magnetization into the x-y plane, where a train of n 180° *RF* refocusing pulses, each separated by an echo time $t_e = 2 \times \tau_2$, is then applied, generating n spin echoes; here, only the magnitude of each echo was acquired (black data point in Fig. 1), producing no chemical shift resolution. The degree of the recovery during time τ_1 is determined by the longitudinal relaxation time constant T_1 and defines the amplitude of the initial echo, while the decay of the echo train depends on the transverse T_2 relaxation of the spin ensemble. A 2D matrix is then constructed by repeating the experiment for several recovery times τ_1.

In this work sixteen logarithmically spaced τ_1 recovery delays were used (between 1 ms and 10 s) and $n = 512$ spin echoes were acquired in a single shot, with an echo time spacing of $t_e = 0.5$ ms. A recycle delay of $5 \times T_1$ was used between each scan to ensure maximal signal was obtained, while sixteen repeat scans were used in order to accommodate the *RF* phase cycle of the NMR pulse sequence and to provide signal averaging to improve the SNR of the acquired data. The duration of each experiment was approximately 30 min.

To obtain the 2D $T_1 - T_2$ distribution, the data must be numerically inverted. The NMR data is described by a Fredholm integral of the first kind [39].

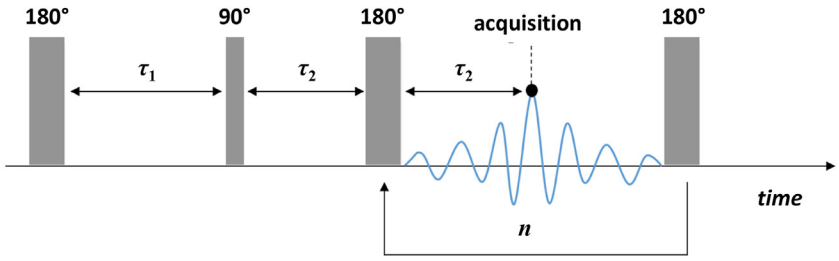

Fig. 1. Schematic of the $T_1 - T_2$ pulse sequence used in this work. The thick vertical bars represents the 180° *RF* pulse and the thin bar the 90° *RF* pulse. The center of the echoes is separated in time by $t_e = 2 \times \tau_2$.

$$\frac{b(\tau_1, nt_e)}{b(0,0)} = \int_{-\infty}^{+\infty}\int_{-\infty}^{+\infty} K(\tau_1, T_1, nt_e, T_2) f(T_1, T_2) dlog(T_1) dlog(T_2) + \varepsilon \quad (1)$$

In Eq. (1) $b(\tau_1, nt_e)/b(0,0)$ is the normalised NMR spin echo signal intensity, ε is the experimental error (noise), $f(T_1, T_2)$ is the required 2D distribution of relaxation time constants, and $K(\tau_1,T_1,nt_e,T_2)$ is the kernel function that represents the expected form of the data, such that:

$$K(\tau_1, T_1, nt_e, T_2) = \left[1 - 2\exp\left(\frac{-\tau_1}{T_1}\right)\right]\exp\left(\frac{-nt_e}{T_2}\right) \quad (2)$$

The first exponent in Eq. (2) describes the T_1 relaxation and the second exponent describes the T_2 relaxation. The kernel function is separable as the two exponents do not share a common time base, which means that for a given set of (τ_1, T_1) the expected behavior of the signal amplitude can be determined separately from the one for a given set of (nt_e, T_2). Using the method described by Venkataramanan et al. [40] the Fredholm integral in Eq. (1) can be solved efficiently in vector-matrix form. In order to obtain a stable distribution in the presence of noise, the Tikhonov regularization was applied [41], with the smoothing parameter amplitude chosen using the generalized cross-validation method [42]. The T_1/T_2 ratio may then be calculated from the logarithmic mean of the individual $T_{1,2}$ dimensions.

2.3. Computational methods

A one-unit-cell siliceous MFI zeolite model with the lattice parameters of a = 20.090 Å, b = 19.738 Å and c = 13.142 Å and $\alpha = \beta = \gamma = 90.0°$ was constructed based on the International Zeolite Association (IZA) database of zeolite structures (http://www.iza-structure.org/databases/). The MFI structure consists of intersectional straight and sinusoidal ten-membered-ring (10 MR) channels and contains 96 silicon and 192 oxygen atoms.

MFI models with atomic silicon-to-aluminium molar ratios of 47, 31, 18.2 and 12.7 (corresponding to the SAR values of 94, 62, 36.4 and 25.4) were constructed based on the one-unit-cell MFI model described above. The locations of the Al atoms in these MFI models were chosen based on the previous literature, suggesting that T1, T2, T3, T9, T11 and T12 sites are the likely positions, which can be easily replaced by Al atoms [43–45]. The corresponding computational models are illustrated in Fig. 2.

Density functional theory (DFT) calculations were carried out using the DMol3 package [46–48] in Accelrys Materials Studio 5.5. The exchange and correlation energy was calculated within the generalized gradient approximation (GGA) using the form of the Perdew-Burke-Ernzerhof functional (PBE) [49]. The structure was optimized until the total energy, force, and displacement were

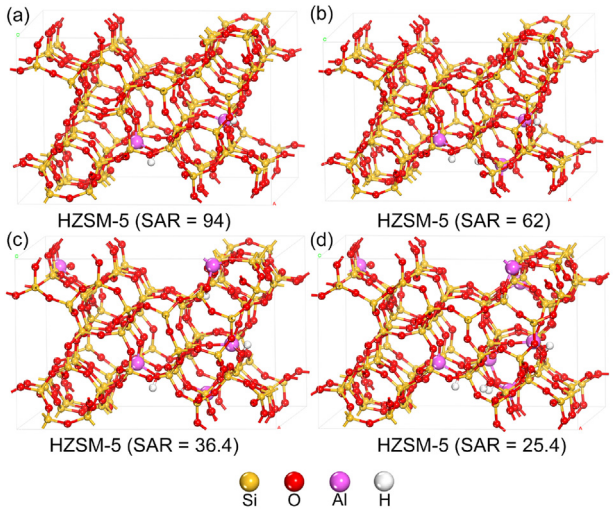

Fig. 2. Optimised structures of HMFI zeolite models with different SAR values of (a) 94, (b) 62, (c) 36.4 and (d) 25.4.

smaller than 1.0×10^{-5} Ha, 2.0×10^{-3} Ha/Å and 5.0×10^{-3} Å, respectively. All atoms in the models were treated with all-electron double numerical basis sets and with polarization (DNP) function.

The adsorption energy (E_{ads}, of probing guest molecules on HZSM-5 porous frameworks) was determined using Eq. (3):

$$E_{ads} = E_{(adsorbate+zeolite)} - (E_{adsorbate} + E_{zeolite}) \quad (3)$$

where $E_{(adsorbate+zeolite)}$, $E_{zeolite}$, $E_{adsorbate}$ are the electronic energy of the adsorbate-zeolite pair, bare zeolite and adsorbate, respectively.

The electron density difference (Δρ, of the probing guest molecules in HZSM-5 frameworks) was determined according to Eq. (4):

$$\Delta\rho = \rho_{AB} - \rho_A - \rho_B \quad (4)$$

where ρ_{AB}, ρ_A, ρ_B are the electron densities of the optimized adsorption structure of AB (host-guest), optimized structure of A (host, i.e., the zeolite model) and optimized structure of B (guest, i.e., the probe molecule), respectively.

3. Results and discussion

3.1. Experimental NMR measurements

A typical set of $T_1 - T_2$ correlation plots for the samples studied in this work is shown in Fig. S1, which reports relaxation data for water adsorbed in HZSM-5 zeolites with SAR values of 23, 30, 50 and 80. Single values of T_1 and T_2 are reported in Fig. S2 and Fig. S3. A summary of the results for water, methanol, toluene and methyl cyclohexane is

shown in Fig. 3, presenting the T_1/T_2 ratio of these species within HZSM-5 as a function of the total aluminium content per unit cell of zeolite (previously estimated by ICP-MS [37]), which corresponds to an equivalent SAR value. We interpret this T_1/T_2 data according to the translational diffusion model of Mitchell and co-workers, which has been successfully utilized to rationalize probe molecule relaxation trends across a range of catalytically active porous solids [16,18,23]. Within this framework, the observed relaxation time ratio is determined by repeated encounters with adsorption sites at the pore surface, with more energetically favorable interactions, i.e., stronger adsorption interactions, leading to larger T_1/T_2 values [23,24]. This interpretation is readily extended to the acidic HZSM-5 zeolites under investigation here, where adsorption at Brønsted acid sites facilitates surface sensitive relaxation phenomena through a reduction in molecular dynamics upon adsorption, and *via* dipolar coupling between surface and adsorbate-bound proton spins [24].

For lower acidity zeolites, that is, higher SAR values of 50 and 80, a comparable strength of surface interaction for all species is observed for all four adsorbate molecules, as evidenced by the T_1/T_2 ratio, which is similar for all species within the margin of the experimental error, i.e., within 5% relative error. This is likely due to the lower number of surface hydroxyls for high SAR values, mainly Brønsted acid sites, which makes the zeolite surface less sensitive to the probe molecules. As the total Al content increases, that is, the SAR decreases and the number of Brønsted acid sites increases [50], the T_1/T_2 values of water and methanol increase significantly, indicating an increased surface affinity, which could be explained by the relatively strong hydrophilicity of HZSM-5 at lower SAR, as reported elsewhere [51]. In contrast, the T_1/T_2 values of toluene and methyl cyclohexane remain relatively small and do not change significantly. We interpret this relaxation behavior as an indication of weaker surface interactions within the HZSM-5 pore network and significantly reduced sensitivity to changes in surface acidity and pore surface chemistry, relative to polar molecules.

The results in Fig. 3 clearly show that for the most acidic zeolite under investigation, HZSM-5 (23), the strength of interaction shows the following pattern:

water > methanol >> toluene > methyl cyclohexane.

This trend suggests that for high acidity HZSM-5 zeolites water has the strongest interaction, followed by methanol, and then

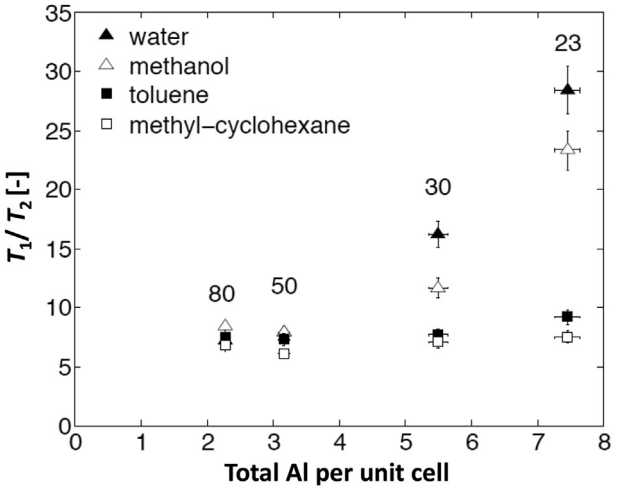

Fig. 3. Ratio of NMR relaxation time constants, T_1/T_2, of water **(filled triangle)**, methanol **(empty triangle),** toluene **(filled square)** and methyl cyclohexane **(empty square)** adsorbed in HZSM-5 with varying SAR values (80, 50, 30 and 23 from left to right).

hydrocarbons, with the latter showing a much weaker pore surface interaction compared to water and methanol. This can be explained by the ability of water and methanol to form strong hydrogen bonding interactions with the surface −OH groups of HZSM-5 with high acidity, whereas hydrocarbons mostly interact through much weaker van der Waals interactions. It is noted that for the HZSM-5 (23) toluene shows an appreciable higher T_1/T_2 value compared to methyl cyclohexane. This may be explained by the ability of toluene to interact with the zeolite surface *via* its aromatic ring, as suggested by previous studies [52]. Thus, the aromatic properties of toluene, in contrast to methyl cyclohexane which has an aliphatic ring, are suggested to contribute to the more pronounced interaction with the HZSM-5 surface.

At this point, it is interesting to note that Nakamoto and Takahashi [51] conducted uptake adsorption studies of HZSM-5 zeolites with different SAR values and observed that as the SAR decreases (i.e., the Al content increases) the uptake for methanol and water increases sharply, whereas for hydrocarbons the profile remains mostly flat. This finding is consistent with the trends reported in Fig. 3, which also show a nearly flat profile for hydrocarbons and a sharp increase for methanol and water. In addition, in their work, for HZSM-5 zeolites with SAR values below 50, the trends reported suggest that water and methanol uptake is going to become much higher than hydrocarbons, which is also consistent with our findings.

In order to further understand and validate the results reported in this work, we have analyzed the T_1/T_2 ratio against the polarity of each molecular species adsorbed over the various HZSM-5 samples with different SAR values. The polarity of a molecule is a measure of its dipole moment, and thus a measure of how effective the molecule acts as a hydrogen bond acceptor [53]. Therefore, the polarity is an important indicator of interaction strength if the adsorption is dominated by hydrogen bonding. Experimentally determined polarity values, relative to water, were taken from the literature [54]. For methyl cyclohexane, to the best of our knowledge, no value of polarity has been reported and the value was approximated to that of cyclohexane, which is a reasonable assumption. Our experimentally acquired T_1/T_2 ratio values are plotted against the respective polarity values for each HZSM-5 (SAR) in Fig. 4, providing a comparison of the adsorption behavior of each probe molecule over each pore surface. The T_1/T_2 ratio of methyl cyclohexane, toluene, methanol and water (from left to right) shows a strong correlation with relative polarity for both the HZSM-5 (23) and HZSM-5 (30) zeolites. Conversely, HZSM-5 samples with higher values of SAR (HZSM-5 (50) and HZSM-5 (80)) shown a very weak-to-no correlation between T_1/T_2 and polarity. This provides another important result, which indicates that hydrophilic HZSM-5 surfaces, that is, low SAR and thus high Al content (i.e., high acidity and high concentration of surface hydroxyls) are more sensitive to the relative polarity of the probe molecules than the more hydrophobic surfaces with high SAR and low Al concentration (low acidity and low concentration of surface hydroxyls).

It is interesting to note that recently reported FFC NMR measurements on alumina-based porous materials have shown that the dependence of the total observable dispersion (TOD) parameter as a function of solvent polarity is similar to that reported for the T_1/T_2 ratio data shown in Fig. 4 [33]. Values of TOD of solvents with different polarity in pores have been reported to be also affected by pore size [34], which can be related to the observed restricted diffusion [55].

4. DFT calculations

To understand the effect of framework Al in HZSM-5 zeolites on the guest-host interaction, molecular modelling was performed at

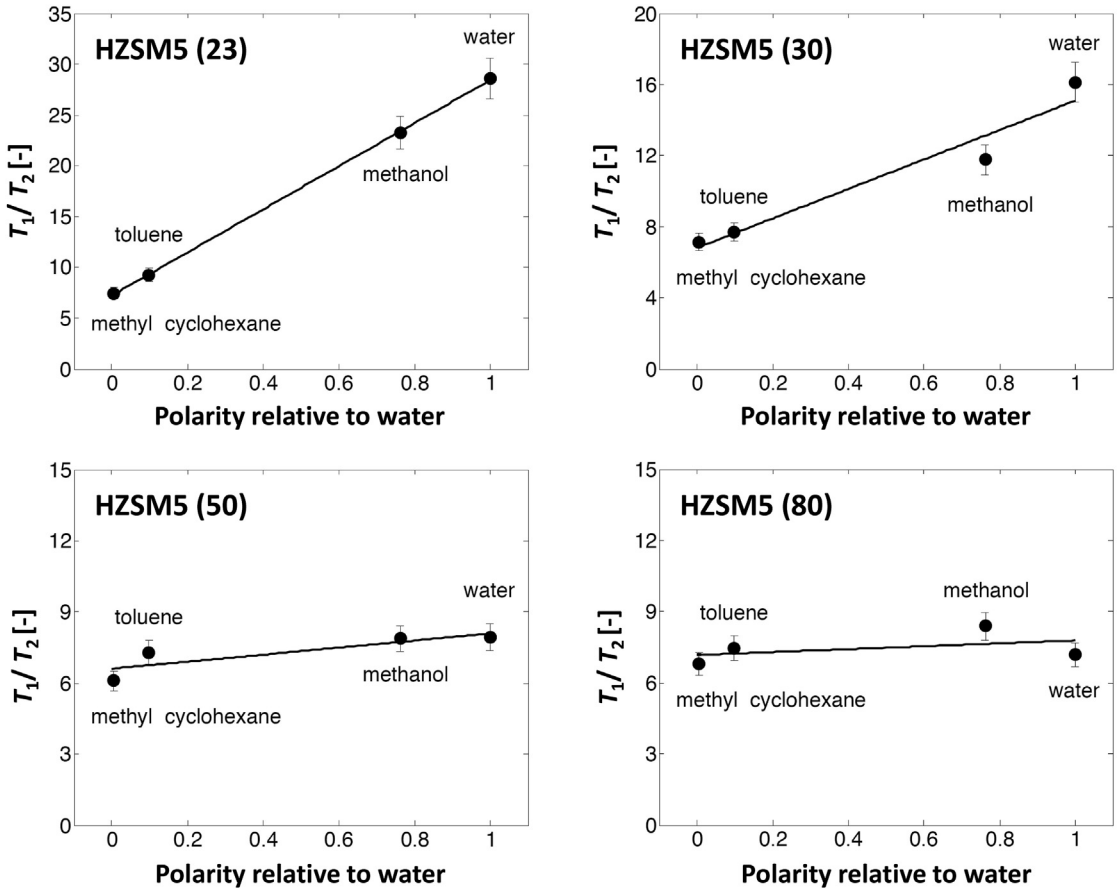

Fig. 4. Correlation of T_1/T_2 values of methyl cyclohexane, toluene, methanol and water (from left to right) adsorbed in HZSM-5 with varying SAR values (23, 30, 50 and 80) against their polarity values relative to water. The solid line represents a fit of a linear equation to data and is used as a guide to the eye.

the electronic level utilizing DFT calculations. Here, water molecules (used as a prototypical polar probe) and toluene molecules (a prototypical non-polar probe) were used to study the interaction between the guest molecules and host zeolite frameworks at the atomic level. The adsorption configurations of water and toluene molecules within ZSM-5 zeolites with different SAR values are shown in Fig. 5. It was predicted that water adsorption on HZSM-5 with high SAR of 94, i.e., low Al concertation, is mainly due to the weak hydrogen bonding (between water molecule and framework oxygen, as shown in Fig. 5a). A decrease in SAR of the zeolites, that is, an increase in Al concentration, leads to an increase of the interaction between water molecules and Brønsted acid sites *via* strong hydrogen bonding (Fig. 5b–d), which agrees with the NMR results and provides mechanistic details on the type of bonding responsible for such enhanced interactions. In addition, the strong guest-host interaction in low SAR HZSM-5 also encouraged strong intermolecular hydrogen bonding between water molecules adsorbed on adjacent Brønsted acid sites, which is exemplified by the case with HZSM-5 of SAR = 36.4 and 25.4, as shown in Fig. 5c and d.

Regarding the cases of toluene, the guest-host interaction in the high SAR zeolites (SAR = 94 and 62, Fig. 5e and f) are mainly due to the weak van der Waals interaction. When the concentration of framework Al increases, that is, the SAR decreases to 36.4 and 25.4, toluene adsorption on either individual −OH groups or two −OH groups located in one 10-membered-ring (10 MR) of HZSM-5 zeolites (as illustrated in Fig. 5g and h) was promoted. The change in molecular adsorption mode between the polar/non-polar guests and the HZSM-5 hosts (with different SAR values) is consistent with the different adsorption characteristics inferred by our experimental NMR data.

The adsorption energy (E_{ads}, Eq. (3)) values of guest molecules (i.e., water and toluene) obtained by DFT calculations are shown in Table 1. Values of the calculated E_{ads} are negative due to the exothermic nature of adsorption processes. The absolute values of E_{ads} for the water-HZSM-5 cases are smaller than that of the toluene-HZSM-5 cases adsorption energy, which suggests stronger binding of toluene with the HZSM-5 frameworks compared to water, being in apparent contradiction to the experimental the NMR data. However, it is worth noting that the calculated adsorption energy is the overall interaction energy, which considers both the electrostatic interaction between the guest molecules and the Brønsted acid sites in zeolites, as well as the dispersion forces exerted by the confining environment on guest molecules (which are unrelated to acid strength of zeolites) [56], which are much more significant in toluene given its larger size compared to water (i.e., ~0.58 nm vs. ~0.265 nm). Therefore, the magnitude of the adsorption energies cannot be the fair criterion to assess the link between the guest molecule interactions and the concentration of Brønsted acid sites (which is related to the SAR of zeolites) within zeolite framework. Similar phenomena were also reported for ammonia and pyridine adsorption on H-FAU zeolite models, in which the absolute E_{ads} values of pyridine are higher than that of NH_3 due to the large molecular size of pyridine, though the basicity of NH_3 is stronger than that of pyridine [57].

In order to show the connection between the electrostatic interaction (between the guest molecules and the Brønsted acid sites in zeolites) and SAR of HZSM-5 zeolites qualitatively, the

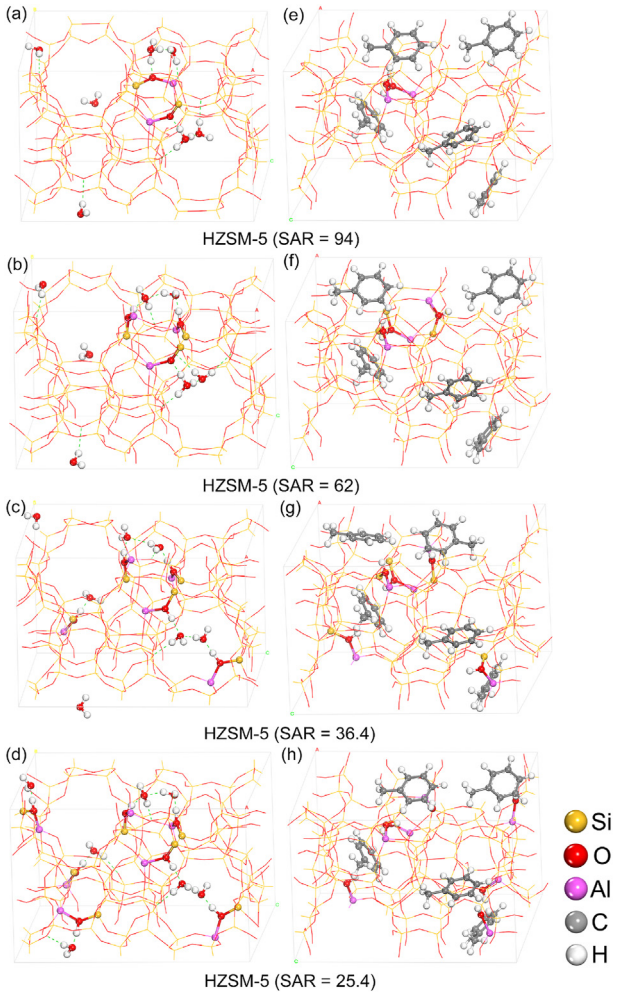

Fig. 5. Adsorption configuration of water (a, b, c, d) and toluene (e, f, g, h) in HZSM-5 frameworks with SAR of 94 (a, e), 62 (b, f), 36.4 (c, g) and 25.4 (d, h).

Table 1
DFT adsorption energy (E_{ads}) of water and toluene molecules within HZSM-5 zeolites with different SAR values.

SAR	$E_{ads,\ water}$ (kJ/mol)	$E_{ads,\ toluene}$ (kJ/mol)
94	−90	−165
62	−95	−179
36.4	−97	−167
25.4	−110	−177

electronic properties and independent gradient model (IGM) for the adsorption of water/toluene molecules on the HZSM-5 with SAR of 94 (as the high SAR model) and 25.4 (as the low SAR model) were visualized and analyzed, as shown in Fig. 6. Fig. 6a–d show the adsorption configurations of the guest molecules (i.e., water and toluene) in the cases of lone Brønsted site and pair Brønsted sites, which are likely to be present in the unit cell of a high SAR HZSM-5 and a low SAR HZSM-5, respectively. The corresponding electron density difference maps and IGM analysis are shown in Fig. 6e–h and 6i-l, respectively. For the adsorption of water on a lone Brønsted site, water interacts with one proton and donates electrons to the site, as shown in Fig. 6a and e, and electrons are concentrated mainly in one region, that is, between the hydrogen atom of the lone Brønsted site and the oxygen atom of water molecule, as indicated by the blue rectangle. With a decrease in the SAR of HZSM-5, i.e., increased number of Brønsted site in the unit cell, guest-host and guest-guest interactions are enhanced (Fig. 6b), which are reflected by the additional accumulation of electrons between the framework oxygen atom and hydrogen atom of water and between the hydrogen atom in water and the oxygen atom in the adjacent water, as shown in Fig. 6f, the blue rectangles. This synergistic guest-host interaction can be explained by the availability of additional Brønsted sites in the unit cell, leading to the strong intermolecular hydrogen bonding between two adjoining adsorbed water molecules, which in turn promotes the additional interaction between the guest-host (i.e., the framework oxygen and hydrogen atom in the adsorbed water).

In the case of toluene adsorption on single Brønsted site, our simulation shows that the adsorbate interacts with hydrogen atom of the Brønsted site and donates π electron density to the site, as seen in Fig. 6c and g. With the additional Brønsted sites, the modelling results suggest that a single toluene may interact with two hydrogen atoms of the Brønsted sites in the pore, one both side of the probe molecule (Fig. 6d and h). Although the strength of guest-host interaction is enhanced due to the increased number of Brønsted sites in the unit cell (i.e., in a low SAR HZSM-5), the individual interaction strength between toluene and one hydrogen atom of the two Brønsted sites is weakened. Furthermore, it is worth noting that in the case of toluene adsorption, toluene-toluene intermolecular interactions do not exist since the pore can accommodate one toluene molecule only, being consistent with the comparatively weak interaction measured for the hydrocarbons and HZSM-5 systems (compared to that for the polar probes and HZSM-5 systems, especially that with low SAR values).

In addition, the findings are verified by IGM analysis as well as shown in Fig. 6i–l. Water molecules are mainly stabilized by H-bond interaction (blue region) and van der Waals interaction (green region) between the oxygen atom of water molecules and hydrogen atom of the Brønsted sites (Fig. 6i and j). Especially, an intermolecular interaction between the two water molecules occurs in the HZSM-5 model containing pair Brønsted sites (as indicated by black rectangular boxes in Fig. 6j), leading to an additional interaction between the framework oxygen atom and hydrogen atom of water (as indicated by pink rectangular boxes in Fig. 6j) and enhancing the guest-host (i.e., polar water molecule-zeolite) interactions. Regarding toluene adsorption, toluene molecules are mainly stabilized by van der Waals interaction between the framework oxygen atoms and hydrogen atoms of toluene (Fig. 6k and l). Although the H-bond interaction between the hydrogen atom of the Brønsted site and C=C (π electrons) of toluene exists, the strong repulsive force (red region) reduces the guest-host (i.e., non-polar toluene molecule-zeolite) significantly, as indicated by black and pink elliptical boxes in Fig. 6k and l.

In summary, the interaction between water and the Brønsted site is significantly stronger than that in the case of toluene adsorption. With a polar probe (of water), as shown in Fig. 6e, f, i and j, it is clear that the higher electron density variation is concentrated near the framework Brønsted acid site(s) (as indicated by red rectangular boxes) and stronger H-bond interactions exist between the water molecules and between the water molecule and the zeolite (as indicated by black and pink rectangular boxes). Conversely, in the cases of non-polar toluene as the adsorption probe, the electron density concentrated more near the aromatic ring (as indicated by blue rectangular boxes in Fig. 6g and h) rather than the Brønsted acid site(s). In particular, there is a strong repulsive interaction between toluene molecule(s) and HZSM-5 models (as indicated by black and pink elliptical boxes in Fig. 6k and l). Overall, the findings obtained from our DFT calculations reveal the role of SAR in determining the adsorption characteristics of probe molecules exhibiting different polarity at an electronic level.

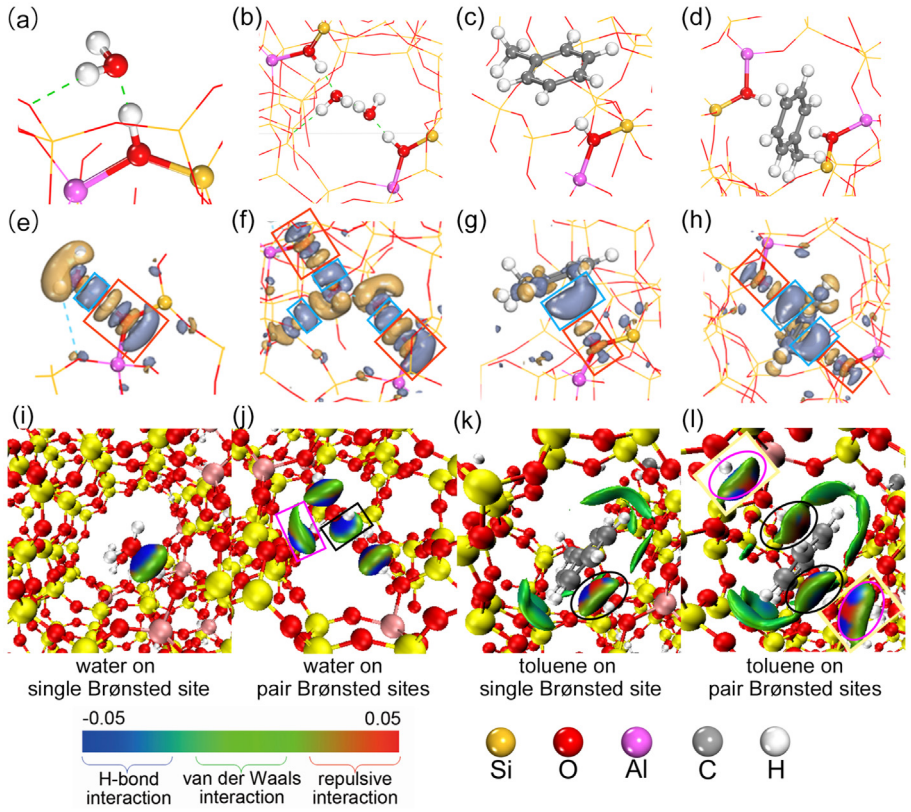

Fig. 6. Detailed view of guest-host adsorption configurations for water (a, b) and toluene (c, d) adsorption on single Brønsted site (a, c) and pair Brønsted sites (b, d) of HZSM-5 zeolites with SAR of 94 and 25.4 (top) and associated electron density difference map (e–h) and independent gradient model (IGM) analysis (i–l) of water (e, f, i, j) and toluene (g, h, k, l) molecules on Brønsted sites of the HZSM-5 zeolites (middle and bottom). Dark grey colour represents the accumulation of electrons, and yellow colour represents the depletion of electrons. (For interpretation of the references to color in this figure legend, the reader is referred to the Web version of this article.)

5. Conclusions

In summary, the findings reported in this work show that the ratio of NMR relaxation time constants T_1/T_2 is a valid indicator for probing adsorbate/adsorbent surface interactions of molecular species in microporous zeolitic materials. We have observed that the T_1/T_2 values of water and methanol, which both exhibit high polarity and ability to form hydrogen bonding, increase with an increase in total Al concentration, which is attributed to an increase in acidity and hence the hydrophilicity of HZSM-5 with low SAR values. In addition, for SAR values of 30 and 23 the T_1/T_2 of water was higher than that for methanol, which suggests a stronger relative interaction with the HZSM-5 surface, and is attributed to the higher polarity of water compared to methanol. The T_1/T_2 values of the low relative polarity hydrocarbons toluene and methyl cyclohexane, for HZSM-5 with low SAR values, are observed to be much smaller relative to those reported for water and methanol in the same samples, which we attribute to the weaker nature of van der Waals interactions with the zeolite surface, compared to the hydrogen bonding interactions that can take place when water or methanol are present. In addition, such values are observed to be less sensitive to the changes in SAR values, and thus to variations in surface hydrophilicity.

Molecular modelling, performed at the electronic level *via* DFT calculations, has been used to explore and contrast the relative surface interaction mechanisms of water and toluene with surface Brønsted sites within model zeolite structures, and to quantify the adsorption energetics of such interactions within materials of varying SAR. Our modelling reveals that water interacts with the zeolite pore surface *via* extensive hydrogen bonding interactions, which increase with decreasing SAR, together with the formation of an intermolecular hydrogen bonding network between water molecules adsorbed on adjacent Brønsted acid sites. Conversely, toluene binds only weakly to the pore surface and does not form an intermolecular network between adsorbed species. The variation in the electron density of water/toluene as a function of decreasing SAR reveals the nature of electrostatic interactions between the guest molecules and host zeolites *via* Brønsted acid sites which is related to SAR of HZSM-5 zeolites.

Overall, the results reported here show that the T_1/T_2 NMR ratio is a useful, non-invasive indicator of surface interactions in microporous zeolites. Furthermore, they show that highly polar molecules able to form hydrogen bonding with the zeolite surface as well, such as water and alcohols, can be a useful probe to characterize microporous zeolite surface acidity through T_1/T_2 NMR relaxation experiments. Our approach represents a useful and more direct alternative to time-consuming and more hazardous experiments, such as TPD measurements using hazardous probe species such as ammonia and pyridine.

Credit author statement

Carmine D'Agostino - Conceptualization; Data curation; Formal analysis; Funding acquisition; Investigation; Methodology; Project administration; Resources; Supervision; Validation; Writing – original draft; Writing – review & editing.

Pierre Bräuer - Conceptualization; Data curation; Formal analysis; Investigation; Methodology; Writing – original draft.

Jian Zheng - Data curation; Formal analysis; Investigation; Methodology; Writing – original draft; Writing – review & editing.

Neil Robinson - Data curation; Formal analysis; Investigation; Methodology; Writing – original draft; Writing – review & editing.

Andrew P.E. York - Data curation; Project administration; Resources; Supervision; Writing – original draft; Writing – review & editing.

Lijuan Song - Data curation; Formal analysis; Investigation; Methodology; Writing – original draft; Writing – review & editing.

Xiaolei Fan - Conceptualization; Data curation; Formal analysis; Investigation; Methodology; Project administration; Resources; Supervision; Writing – original draft; Writing – review & editing.

Declaration of competing interest

The authors declare that they have no known competing financial interests or personal relationships that could have appeared to influence the work reported in this paper.

Data availability

Data will be made available on request.

Acknowledgements

The authors would like to acknowledge Johnson Matthey for sponsoring this work and Prof. Lynn Gladden, University of Cambridge, for allowing access to the NMR facilities. Carmine D'Agostino and Xiaolei Fan would also like to acknowledge the EPSRC (grant no. EP/V026089/1) for funding the research.

Appendix A. Supplementary data

Supplementary data to this article can be found online at https://doi.org/10.1016/j.mtchem.2023.101443.

References

[1] M.O. Daramola, A.J. Burger, M. Pera-Titus, A. Giroir-Fendler, S. Miachon, J.-A. Dalmon, L. Lorenzen, Asia Pac. J. Chem. Eng. 5 (2010) 815–837.
[2] S.J. Raynes, R.A. Taylor, Sustain. Energy Fuels 5 (2021) 2136–2148.
[3] M. Conte, B. Xu, T.E. Davies, J.K. Bartley, A.F. Carley, S.H. Taylor, K. Khalid, G.J. Hutchings, Micro. Meso. Mater. 164 (2012) 207–213.
[4] J.A. Lercher, V. Veefkind, K. Fajerwerg, Vib. Spectrosc. 19 (1999) 107–121.
[5] P. Brauer, O. Situmorang, P.L. Ng, C. D'Agostino, Phys. Chem. Chem. Phys. 20 (2018) 4250–4262.
[6] C. LeMinh, R.A. Jones, I.E. Craven, T.C. Brown, Energy Fuels 11 (1997) 463–469.
[7] A.M. Camiloti, S.L. Jahn, N.D. Velasco, L.F. Moura, D. Cardoso, Appl. Catal. Gen. 182 (1999) 107–113.
[8] S.B. Sharma, B.L. Meyers, D.T. Chen, J. Miller, J.A. Dumesic, Appl. Catal. Gen. 102 (1993) 253–265.
[9] D.J. Parrillo, R.J. Gorte, J. Phy. Chem 97 (1993) 8786–8792.
[10] O.A. Abdelrahman, K.P. Vinter, L. Ren, D. Xu, R.J. Gorte, M. Tsapatsis, P.J. Dauenhauer, Catal. Sci. Technol. 7 (2017) 3831–3841.
[11] L.F. Gladden, J. Mitchell, New J. Phys. 13 (2011) 46.
[12] J.P. Korb, New J. Phys. 13 (2011) 26.
[13] C. D'Agostino, M.D. Mantle, L.F. Gladden, G.D. Moggridge, Chem. Eng. Sci. 74 (2012) 105–113.
[14] C. D'Agostino, S. Chansai, I. Bush, C. Gao, M.D. Mantle, C. Hardacre, S.L. James, L.F. Gladden, Catal. Sci. Technol. 6 (2016) 1661–1666.
[15] N. Robinson, E.F. May, M.L. Johns, ACS Appl. Mater. Interfaces 13 (2021) 54476–54485.
[16] D. Weber, J. Mitchell, J. McGregor, L.F. Gladden, J. Phys. Chem. C 113 (2009) 6610–6615.
[17] C. D'Agostino, G.L. Brett, P.J. Miedziak, D.W. Knight, G.J. Hutchings, L.F. Gladden, M.D. Mantle, Chem. Eur J. 18 (2012) 14426–14433.
[18] J. Mitchell, L.M. Broche, T.C. Chandrasekera, D.J. Lurie, L.F. Gladden, J. Phys. Chem. C 117 (2013) 17699–17706.
[19] G. Di Carmine, D. Ragno, A. Massi, C. D'Agostino, Org. Lett. 22 (2020) 4927–4931.
[20] G. Filippini, F. Longobardo, L. Forster, A. Criado, G. Di Carmine, L. Nasi, C. D'Agostino, M. Melchionna, P. Fornasiero, M. Prato, Sci. Adv. 6 (2020), eabc9923.
[21] B. Zhou, P. Yang, G. Ferrante, M. Pasin, R. Steele, V. Bortolotti, J.-P. Korb, Energy Fuels 33 (2019) 1016–1022.
[22] A. Nagmutdinova, L. Brizi, P. Fantazzini, V. Bortolotti, Appl. Magn. Reson. 52 (2021) 1767–1785.
[23] C. D'Agostino, J. Mitchell, M.D. Mantle, L.F. Gladden, Chem. Eur J. 20 (2014) 13009–13015.
[24] N. Robinson, C. Robertson, L.F. Gladden, S.J. Jenkins, C. D'Agostino, Chem. Phys. Chem. 19 (2018) 2472–2479.
[25] C. D'Agostino, R.D. Armstrong, G.J. Hutchings, L.F. Gladden, ACS Catal. 8 (2018) 7334–7339.
[26] C. D'Agostino, G. Brett, G. Divitini, C. Ducati, G.J. Hutchings, M.D. Mantle, L.F. Gladden, ACS Catal. 7 (2017) 4235–4241.
[27] C. D'Agostino, M.R. Feaviour, G.L. Brett, J. Mitchell, A.P.E. York, G.J. Hutchings, M.D. Mantle, L.F. Gladden, Catal. Sci. Technol. 6 (2016) 7896–7901.
[28] C. D'Agostino, T. Kotionova, J. Mitchell, P.J. Miedziak, D.W. Knight, S.H. Taylor, G.J. Hutchings, L.F. Gladden, M.D. Mantle, Chem. Eur J. 19 (2013) 11725–11732.
[29] A.T. Krzyżak, I. Habina, Micro. Meso. Mater. 231 (2016) 230–239.
[30] Z.T. Lalowicz, A. Birczyński, A. Krzyżak, J. Phys. Chem. C 121 (2017) 26472–26482.
[31] E.V. Silletta, M.I. Velasco, C.G. Gomez, M.C. Strumia, S. Stapf, C. Mattea, G.A. Monti, R.H. Acosta, Langmuir 32 (2016) 7427–7434.
[32] S. Stapf, R. Kimmich, R. Seitter, Phys. Rev. Lett. 75 (1995) 2855–2858.
[33] J. Ward-Williams, J.P. Korb, L.F. Gladden, J. Phys. Chem. C 122 (2018) 20271–20278.
[34] L.G. Linck, S.A. Maldonado Ochoa, M. Ceolín, H. Corti, G.A. Monti, F.V. Chávez, R.H. Acosta, Micro. Mesoporous Mater. 305 (2020), 110351.
[35] N. Robinson, P. Bräuer, A.P.E. York, C. D'Agostino, Phys. Chem. Chem. Phys. 23 (2021) 17752–17760.
[36] C. D'Agostino, A.P.E. York, P. Bräuer, Mater. Today Chem. 24 (2022), 100901.
[37] P. Bräuer, P.L. Ng, O. Situmorang, I. Hitchcock, C. D'Agostino, RSC Adv. 7 (2017) 52604–52613.
[38] Y.Q. Song, L. Venkataramanan, M.D. Hurlimann, M. Flaum, P. Frulla, C. Straley, J. Magn. Reson. 154 (2002) 261–268.
[39] J. Mitchell, T.C. Chandrasekera, L.F. Gladden, Prog. Nucl. Magn. Reson. Spectrosc. 62 (2012) 34–50.
[40] L. Venkataramanan, Y.Q. Song, M.D. Hurlimann, IEEE Trans. Signal Process. 50 (2002) 1017–1026.
[41] G. Wahba, Y. Wang, Commun. Stat. Theor. Methods 19 (1990) 1685–1700.
[42] G.H. Golub, M. Heath, G. Wahba, Technometrics 21 (1979) 215–223.
[43] D.H. Olson, N. Khosrovani, A.W. Peters, B.H. Toby, J. Phys. Chem. B 104 (2000) 4844–4848.
[44] A. Ghorbanpour, J.D. Rimer, L.C. Grabow, Catal. Commun. 52 (2014) 98–102.
[45] B. Xing, J. Ma, R. Li, H. Jiao, Catal. Sci. Technol. 7 (2017) 5694–5708.
[46] B. Delley, J. Chem. Phys. 92 (1990) 508–517.
[47] B. Delley, J. Phy. Chem 100 (1996) 6107–6110.
[48] B. Delley, J. Chem. Phys. 113 (2000) 7756–7764.
[49] J.P. Perdew, K. Burke, M. Ernzerhof, Phys. Rev. Lett. 77 (1996) 3865.
[50] X. Zhu, S. Liu, Y. Song, L. Xu, Appl. Catal. Gen. 288 (2005) 134–142.
[51] H. Nakamoto, H. Takahashi, Zeolites 2 (1982) 67–68.
[52] R. Méndez-Román, N. Cardona-Martínez, Catal. Today 40 (1998) 353–365.
[53] J.M. Berg, J.L. Tymoczko, L. Stryer, Biochemistry, W. H. Freeman, New York, 2002.
[54] C. Reichardt, T. Welton, Solvents and Solvent Effects in Organic Chemistry, Wiley-VCH, Weinheim, Germany, 2011.
[55] I.J. Chevallier-Boutell, G.A. Monti, H. Corti, J.A. Olmos-Asar, M.B. Franzoni, R.H. Acosta, Micro. Meso. Mater. 326 (2021), 111315.
[56] A.J. Jones, E. Iglesia, ACS Catal. 5 (2015) 5741–5755.
[57] C. Liu, G. Li, E.J.M. Hensen, E.A. Pidko, J. Catal. 344 (2016) 570–577.